Surface & Coatings Technology 491 (2024) 131166

Contents lists available at ScienceDirect

Surface & Coatings Technology

journal homepage: www.elsevier.com/locate/surfcoat

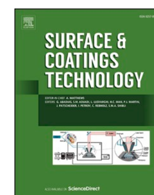

Full Length Article

Arc-enhanced glow discharge ion etching of WC-Co cemented carbide for improved PVD thin film adhesion and asymmetric cutting edge preparation of micro milling tools

Nelson Filipe Lopes Dias [a,*], Alexander Leonard Meijer [b,*], Christoph Paul Jäckel [b], Alexander Frisch [a], Dirk Biermann [b], Wolfgang Tillmann [a]

[a] Institute of Materials Engineering, TU Dortmund University, Leonhard-Euler-Straße 2, 44227 Dortmund, Germany
[b] Institute of Machining Technology, TU Dortmund University, Baroper Str. 303, Dortmund 44227, Germany

A R T I C L E I N F O

Keywords:
Ion etching
Pretreatment
Cemented carbide
Magnetron sputtering
TiAlSiN
Micromilling

A B S T R A C T

Wear-resistant thin films on cutting tools require effective ion etching to enhance adhesion and thus extended tool service life. Arc enhanced glow discharge (AEGD) ion etching, characterized by high ionization degrees and high etch rates, was applied to ultrafine-grained WC-Co cemented carbide, commonly used for micromilling cutters. The effect of AEGD ion etching on the surface integrity of WC-Co and the resulting adhesion behavior of a TiAlSiN thin film was investigated by varying the etching time in comparison with conventional glow discharge (GD) ion etching. In addition, the impact of intensive etching on the cutting edge geometry of micro end cutters and, in turn, on the cutting performance in micromilling of hardened and annealed high-speed steel was evaluated.

AEGD achieves remarkable etch rates of 12 nm/min at extended etching times, which are 100 times greater than conventional glow discharge (GD) ion etching. Prolonged AEGD ion etching for ≥30 min removes entire near-surface WC grains and exposes carbides beneath, resulting in increased surface roughness. After the etching process, polished WC-Co substrates exhibit a slight reduction in residual compressive stresses, which steadily decrease with increasing AEGD ion etching time. Furthermore, a TiAlSiN thin film demonstrates high adhesion on AEGD-etched surfaces compared to GD ion etching. Even a brief 5 min AEGD ion etching ensures the highest adhesion class according to the Rockwell C indentation test. Moreover, the intensive material removal results in significant changes in cutting edge geometry of micro end cutters, yielding substantial cutting edge rounding and an asymmetrical shape with form-factors $K \geq 2$. In cutting tests, the resulting cutting edge geometries effectively reduce the wear formation and the associated wear-related increase in process forces during micromilling hardened and tempered powder metallurgical high-speed steel. In summary, AEGD ion etching emerges as a highly effective method for both enhancing thin film adhesion and preparing adapted asymmetrical cutting edge geometries for micromilling tools.

1. Introduction

In advanced machining processes, an adjusted combination of pretreatments of cutting tools and the subsequent application of a wear-resistant thin film is highly relevant for enhancing the cutting performance and extending the service life of coated tools [1]. This is especially important in micromachining, where the tool pretreatment is critical to fully exploit the potential of the applied thin films [2–4]. Micromilling, for instance, is a highly effective method for achieving high accuracy in dimensions and shapes, making it a promising machining process for die and mold manufacturing [5]. Furthermore, micromilling induces residual compressive stresses within the subsurface zone of the tool steel [6,7]. This not only enhances fatigue resistance but also promotes improved adhesion of a subsequent protective thin film to the steel tool [7,8]. Micromilling cutters are typically made of ultrafine-grained WC-Co cemented carbide with an average WC grain size ranging from 0.2 and 0.5 μm [9]. In comparison to WC-Co cemented carbides with submicron grains of 0.5 to 0.9 μm or fine

* Corresponding authors.
E-mail addresses: filipe.dias@tu-dortmund.de (N.F. Lopes Dias), alexander.meijer@tu-dortmund.de (A.L. Meijer).

https://doi.org/10.1016/j.surfcoat.2024.131166
Received 15 May 2024; Received in revised form 4 July 2024; Accepted 20 July 2024
Available online 22 July 2024
0257-8972/© 2024 The Authors. Published by Elsevier B.V. This is an open access article under the CC BY license (http://creativecommons.org/licenses/by/4.0/).

grains of 1.0 to 1.3 μm, ultrafine-grained WC-Co cemented carbides exhibit higher hardness and bending strength [10]. In addition, small cutting edge radii below 1 μm can be achieved due to the small grain size [11].

Wear-resistant thin films are commonly applied to micromilling cutters through physical vapor deposition (PVD) processes [12]. Achieving high adhesion on the cutting edge is essential to fully exploit the potential of PVD thin films [13]. In addition to traditional mechanical pretreatments, such as tumbling, brushing, or blasting [3,4], ion etching serves as a physicochemical pretreatment and is commonly employed to prepare the tool's surface before the PVD process [14]. Its notable advantage over alternative pretreatment processes lies in its applicability within the deposition chamber, allowing for immediate implementation just before the PVD coating process [15]. Etching with highly energetic noble gas ions not only efficiently removes impurities and oxides from the substrate surface but also enhances the chemical bonds between the substrate atoms and the condensing atoms of the growing PVD thin film [16]. For cemented carbides, ion etching also ensures the removal of smeared Co layer from the tool's surface, which may be formed during mechanical pretreatments, such as grinding or honing [17].

In glow discharge (GD) ion etching, a plasma is generated by exposing the noble gas, typically argon (Ar), within the deposition chamber to a voltage exceeding the breakdown voltage of the respective noble gas, thereby ionizing it [18]. The simplest variant involves applying a negative direct current (dc) voltage to the substrates to ionize the noble gas and accelerate the noble gas ions onto the substrates [19]. Alternatively, GD ion etching can be conducted using a pulsed bias voltage with mid-frequency (mf) or radio-frequency [20]. The advantage of employing a pulsed bias voltage in GD ion etching is the prevention of charge build-up, especially when etching thick oxide layers from substrate's surface with reduced electrical conductivity [21]. In industrial applications, the use of GD ion etching with a mf-pulsed bias voltage is a well-established technique for pretreating substrates before the PVD process [22]. However, GD ion etching is characterized by relatively modest etch rates attributed to the low plasma density [16]. For WC-Co cemented carbides, ion etching selectively removes the Co binder phase to a greater extent than the WC grains [23]. This discrepancy is due to the higher sputtering yield of Co compared to WC, which leads to a more pronounced exposure of the WC grains on the surface. As a result, GD ion etching typically results in increased surface roughness, thereby improving the adhesion through mechanical interlocking at the interface between the substrate and thin film [24,25].

Advanced GD ion etching processes aim to increase the etch rate by enhancing the plasma density. Various methods are employed for this purpose, with certain ion etching techniques generating electrons to rise the ionization degree of the noble gas. Hot filaments or hollow cathodes are commonly used as electron sources, while an anode attracts the electrons towards the substrate carousel to augment the noble gas ionization through electron collision [20]. Gassner et al. investigated the effect of an intensive ion etching on cutting inserts made of fine-grained WC-Co cemented carbides [26]. Although the ion etching technique was not specified in their study, the PVD equipment used is known to employ a hot filament and an auxiliary anode, positioned both above and below the center of the substrate carousel, as described in the corresponding patent of the PVD equipment manufacturer [27]. Gassner et al. reported that extended etching time and an elevated bias voltage significantly contribute to preferential sputtering of the Co binder phase. This results in exposing the WC grains to the surface with rounded edges, consequently increasing the surface roughness. They measured an etch rate of (8 ± 1) nm/min for the fine-grained WC-Co cemented carbides at a bias voltage of −185 V with a linear increase in material removal over time from 220 nm after 20 min to 930 nm after 80 min.

Another promising method to enhance plasma density during ion etching is achieved by an arc enhanced glow discharge (AEGD) [28]. In AEGD ion etching, a cathodic arc evaporator equipped with a Ti target is positioned in front of a shutter. It deposits material onto the shutter plate by arc evaporation. During this process, a significant number of electrons are generated through the ionization of the target material. These electrons are then attracted through a gap between AEGD module and shutter towards the substrate carousel by an additional electric field created by an anode rod or anodically switched arc evaporators adjacent to the AEGD module. These electrons contribute to a higher ionization degree of the noble gas Ar through inelastic collisions [29]. The resulting elevated plasma density with ionized noble gas leads to high etch rates and improves the adhesion of the thin film to the substrate material.

In a previous work by the authors, AEGD ion etching was employed to pretreat micro end mills of ultrafine-grained WC-Co cemented carbide [30]. The study demonstrated that extended etching times and elevated bias voltages contribute to significant material removal and increased roughness, resulting in enhanced adhesion of a titanium aluminum nitride (TiAlN) thin film on the WC-Co cemented carbide. Notably, the intensive etching process produced an asymmetrical cutting edge geometry with a form-factor K ranging between 2.0 and 2.4. Furthermore, varying the etching time resulted in different average cutting edge roundings $\overline{S}$. The considerable asymmetry of the cutting edge geometry achieved, which can only be produced to a limited extent in the desired size range ($\overline{S} < 8$ μm) using mechanical preparation processes, enabled a significant improvement in process performance and wear resistance. The process approach described for cutting edge preparation of precision end mills with a diameter of 1 mm thus overcomes the technological limits of established mechanical preparation processes. This highlights the promising potential of AEGD ion etching in the pretreatment of cutting tools.

Nevertheless, the mechanism underlying the etching removal of ultrafine-grained WC-Co cemented carbide by AEGD ion etching, and its distinction from conventional GD etching, remains unclear. This is because a direct comparison between AEGD and conventional GD ion etching on ultrafine-grained WC-Co cemented carbide has not been conducted so far. Therefore, this type of cemented carbide underwent etching with varying durations in steps of 5, 15, 30, 60, and 120 min using both methods. Etch rates were determined and the impact of both ion etching methods on topographical structure, roughness, and residual stress state of the WC-Co cemented carbide as well as the adhesion of a titanium aluminum silicon nitride (TiAlSiN) thin film was analyzed. Furthermore, the results obtained from the cutting edge preparation by AEGD ion etching in a previous study [30] were employed to explore the mechanisms behind asymmetric cutting edge rounding and the subsequent cutting performance of the coated micro end mills.

2. Experimental details

2.1. Ion etching pretreatments and deposition process

The ultrafine-grained WC-Co cemented carbide of type HB20UF (Boehlerit GmbH & Co.KG, Austria) served as material for coin-shaped substrates and for the micro end mills. According to the manufacturer, the utilized cemented carbide contains 92 wt.-% WC and 8 wt.-% Co and possesses a hardness of 1975 HV and a bending strength of 3500 N/mm^2 [31]. The coin-shaped substrates, with a diameter of 20 mm and a height of 4 mm, were metallographically prepared by lapping and polishing. The micro end mills, with a diameter of $D = 1$ mm and a corner radius of $r_\varepsilon = 50$ μm, were derived from the Peakcook Series 599 (Zecha Hartmetall-Werkzeugfabrikation GmbH, Germany). The coin-shaped substrates were positioned on the substrate carousel at a height ranging from 650 to 750 mm relative to the floor of the deposition chamber. The tool holder was set at a height of 600 mm, thereby positioning the cutting edge of the micro end mills at approximately 680 mm.

The GD and AEGD ion etching procedures as well as the PVD process for the TiAlSiN thin film were carried out using a customized PVD device METAPLAS.DOMINO kila flex (Oerlikon Balzers Coating Germany

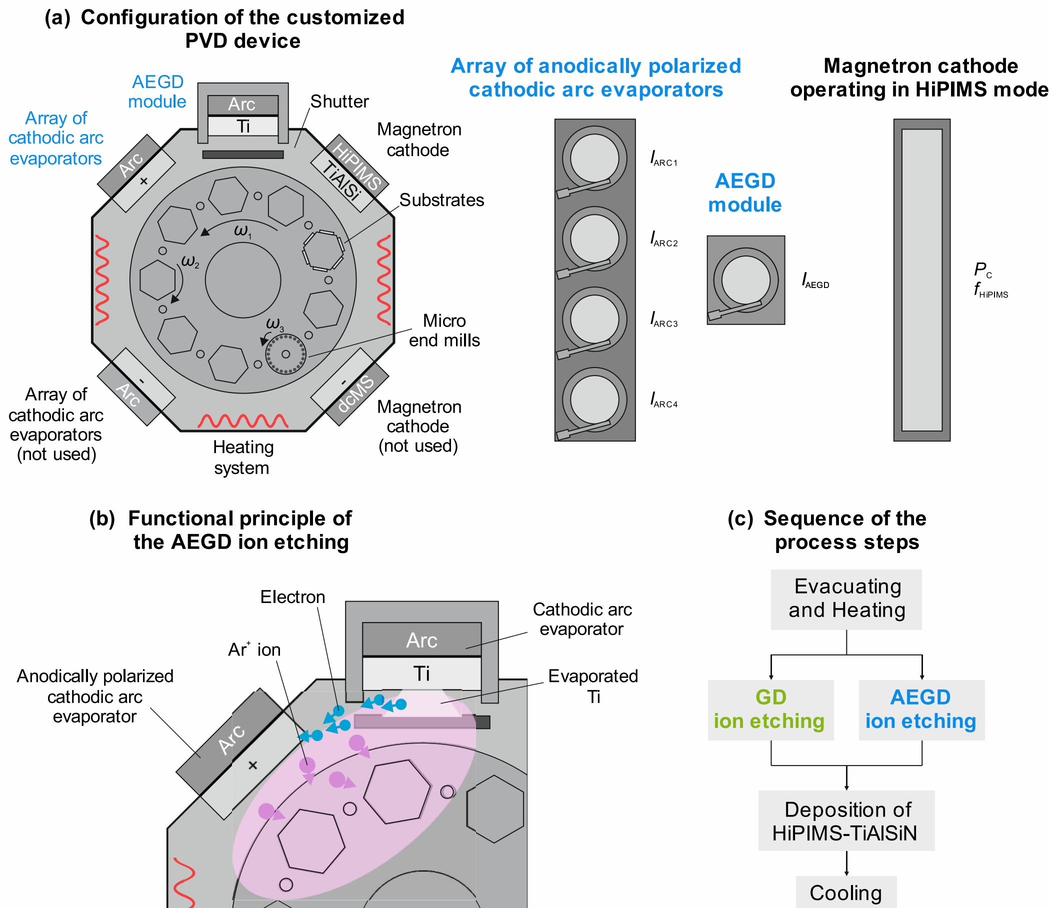

Fig. 1. (a) Configuration of the customized PVD device for AEGD ion etching and deposition of HiPIMS-TiAlSiN, (b) functional principle of the AEGD ion etching, and (c) sequence of the process steps.

GmbH, Germany). Fig. 1a shows the configuration of the PVD device comprising two arrays of four cathodic arc evaporators, two magnetron cathodes, and the AEGD module. The center point of the AEGD module is positioned at a height of 550 mm relative to the floor. The substrates and micro end mills were affixed to the substrate carousel with two-fold and three-fold rotations, respectively. The chamber was evacuated to a base pressure below $p < 4 \times 10^{-5}$ mbar and heated twice for one hour each to degas the deposition chamber and heat the substrates.

Subsequently, either the GD or AEGD ion etching process was conducted. For both procedures, the heater temperature was maintained at $T = 500$ °C and the working pressure was set to $p = 0.01$ mbar (1 Pa) by regulating the Ar gas flow rate. In GD ion etching, the applied bias voltage was pulsed at $U_b = -650$ V with a mid-frequency of $f = 20$ kHz and a duty cycle of 80 %. The level of the applied bias voltage is commonly employed in industrial PVD devices for GD ion etching [32–34]. In advanced AEGD ion etching, the shielded arc evaporator was equipped with a Ti target and operated at a current of $I_{AEGD} = 150$ A. The current of the array of four anodically polarized arc evaporators was $I_{ARC1} = 45$ A, $I_{ARC2} = 35$ A, $I_{ARC3} = 35$ A, and $I_{ARC4} = 45$ A from top to bottom in order to attract the generated electrons during the evaporation of Ti towards the substrate carousel. The higher external currents ensure the uniform attraction of electrons to the four anodically polarized arc evaporators, leading to an even distribution of the plasma on the substrate carousel. The bias voltage was set to $U_b = -300$ V and was also pulsed at 20 kHz with a duty cycle of 80 %. The current of the arc evaporators and the bias voltage were gradually ramped over 11 min to reach the chosen levels. During the etching processes, an average bias current of $I_{GD} = 0.17$ A for GD ion etching and a significantly higher bias current of $I_{AEGD} = 10.22$ A for AEGD ion etching was measured on the substrate carousel in clean, uncoated condition. Given the approximate surface area of 16,000 cm^2 of the substrate planetary, which includes tool holders and dummy towers, these currents correspond to current densities of 0.0106 mA/cm^2 and 0.6388 mA/cm^2, respectively. The temperature on the substrate carousel, measured using a ratio pyrometer, was found to be $T_{GD} = 320$ °C for GD and $T_{AEGD} = 350$ °C for AEGD. Etching time was varied in steps of 5, 15, 30, 60, and 120 min for both GD and AEGD ion etching. The functional principle of AEGD ion etching is schematically illustrated in Fig. 1b.

The deposition of the TiAlSiN thin film was performed using the high-power impulse magnetron sputtering (HiPIMS) technique. The magnetron cathode, operating in HiPIMS mode, was equipped with a $Ti_{42.5}Al_{42.5}Si_{15}$ target with a dimension of 906 × 81 mm^2 (Plansee SE, Germany). The cathode power was set to $P_c = 10$ kW and pulsed with a pulse duration of $t_{on} = 60$ μs and an off-time of $t_{off} = 1000$ μs, resulting in a HiPIMS frequency of approximately $f_{HiPIMS} \approx 940$ Hz. Both process gas Ar and reactive gas N_2 were injected directly in front of the targets through gas lances, with gas flow rates set to $q_{Ar} = 160$ sccm and to $q_{N2} = 60$ sccm. The heating system was adjusted to maintain an approximate substrate temperature of $T = 350$ °C. Throughout the entire deposition process, a dc bias voltage U_b was gradually applied to the substrate holder system, starting at −60 V, then increased stepwise to −100 V, and finally to −140 V. The deposition time was adjusted to obtain a target thickness of 2.5 μm. The HiPIMS-TiAlSiN thin film exhibits a chemical composition of (18.1 ± 0.1) at.-% Ti, (23.4 ± 0.2) at.-% Al, (9.4 ± 0.1) at.-% Si, and (49.2 ± 0.5) at.-% N. The corresponding hardness and elastic modulus were measured as $H = (29.6 \pm 2.1)$ GPa and $E = (325.7$

1. Polished WC-Co surface

2. Application of masking agent

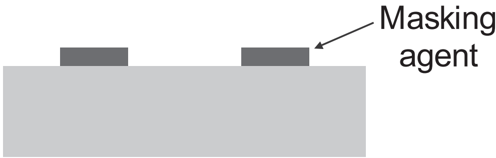

3. Etching of masked WC-Co surface

4. Removal of masking agent

Fig. 2. Schematic illustration showing the method used to determine the material removal after the etching process.

± 25.3) GPa, respectively. The complete process, including both the ion etching procedures and deposition of the HiPIMS-TiAlSiN thin film, is depicted in Fig. 1c.

2.2. Characterization of the etched WC-Co cemented carbide and thin film properties

The topography was analyzed using a field emission scanning electron microscope (SEM) JSM 7001F (JEOL Ltd., Japan). SEM micrographs were taken at specific points on the surface before and after etching, which were marked with hardness indentations to locate them after etching. Additionally, 3D surface images were obtained using a confocal white light interferometer WAFERinspect (confovis GmbH, Germany) to determine the surface roughness. A total of 4 measurements were performed within a measuring range of 430 × 460 μm^2. The mean arithmetic roughness *Sa* was determined from the 3D surface images according to DIN EN ISO 25178-2:2023–09 [35]. A robust Gaussian filter with a nesting index filter of $\lambda_C = 80$ μm was utilized to assess the areal roughness parameters following the specifications outlined in DIN EN ISO 25178-3:2012-11 [36].

To determine the material removal during the etching processes, two straight lines of Nicrobraz Stop-Off Green (Wall Colmonoy Limited, United Kingdom) were applied to the surface of the WC-Co cemented carbides before etching. This material is a surface protection that prevents the adhesion of soldering material but is also used as a masking agent during thermal spraying. In this case, the masking material was used to act as a local etching mask on the WC-Co cemented carbides. The surrounding areas were etched, creating a plateau on the surface of the substrate. Following the etching process, the masking material was removed using ethanol. Four measurements were conducted per substrate to determine the arithmetic mean value for the step height, corresponding to the depth of the material removal. This allowed the calculation of the GD and AEGD ion etching processes. Fig. 2 illustrates the sequential steps involved in the method used to determine the material removal.

The crystallographic structure was examined using x-ray diffraction (XRD) on the D8 Advance diffractometer (Bruker AXS GmbH, Karlsruhe, Germany). The instrument was equipped with a polycapillary parallel x-ray lens of 2 mm and a LynxEye silicon strip detector (Bruker AXS GmbH, Karlsruhe, Germany). The XRD measurements were conducted with Co Kα radiation ($\lambda = 0.17902$ nm) at an acceleration voltage of $U =$ 40 kV and a current of $I = 40$ mA. XRD diffractograms were acquired in Bragg-Brentano geometry over a scanning range of 2θ within 30° and 130° with a scan step of $\Delta 2\theta = 0.035°$ and an exposure time of $\Delta t = 1$ s. The residual stresses in the near-surface region were determined using the $\sin^2\psi$ method for the WC(112) plane, employing x-ray elastic constants provided by Eigenmann and Macherauch [37]. The measurement was conducted over a 2θ range from 122.2° to 125.8° with a step size of $\Delta 2\theta = 0.1°$ and a measuring time of $t = 2$ s. This configuration resulted in a maximum penetration depth of the Co Kα radiation of $z_0 = 1.3$ μm [37].

The adhesion of the TiAlSiN thin films on the etched WC-Co cemented carbide substrates were evaluated using the Rockwell indentation test in accordance with DIN 4856:2018–02 [38]. For WC-Co cemented carbide substrates, the Rockwell scale A with a test force of 60 kp was employed. Three indents were made on each TiAlSiN-coated substrate and then examined using SEM to assign each to one of the six adhesion classes. Based on the adhesion classes, a qualitative assessment of the adhesive behavior of the TiAlSiN thin film was conducted. Adhesion classes HF1 to HF4 indicate an acceptable adhesive strength for industrial applications, while HF5 to HF6 indicate an unacceptable adhesive strength.

The cutting edge geometry of the etched micro end mills was characterized using the form-factor method, which includes parameters the cutting edge segment on the flank face S_α and on the rake face S_β as well

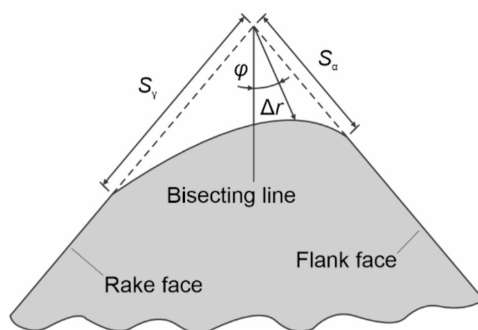

Fig. 3. Parameters of the form-factor method to describe the cutting edge geometry (adapted from [48]).

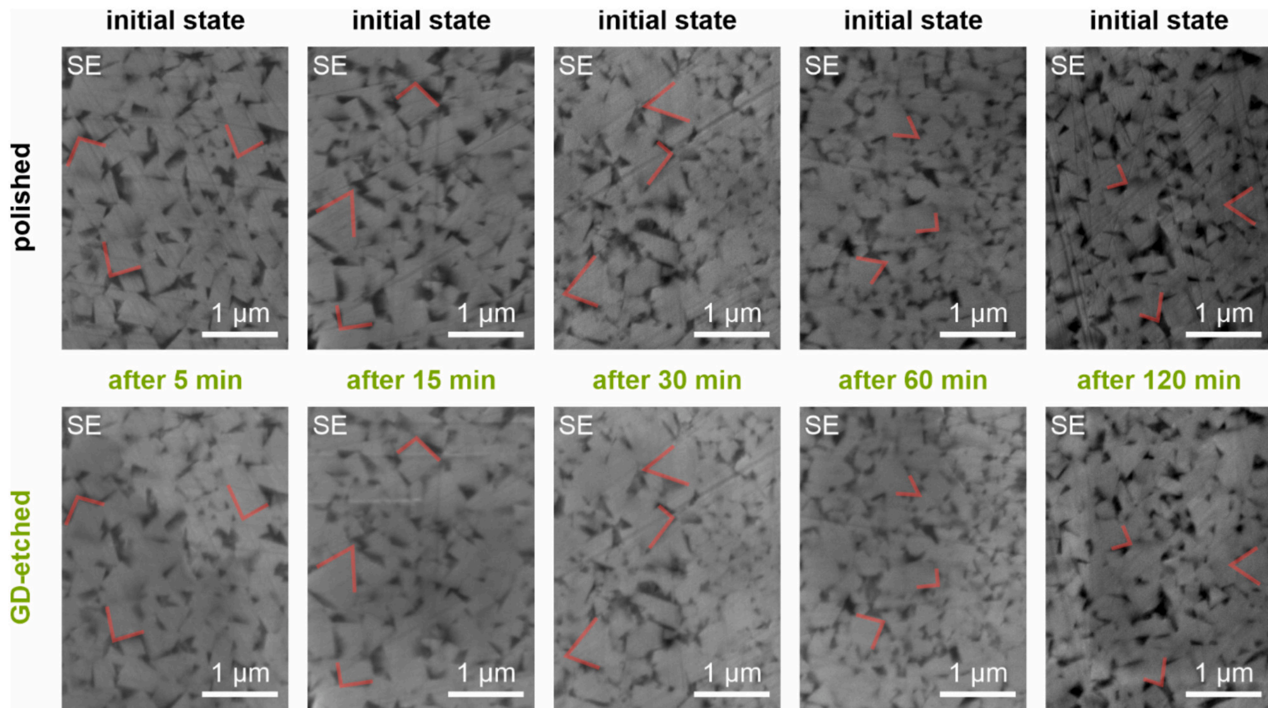

Fig. 4. SEM micrographs of the surface of the ultrafine-grained WC-Co cemented carbide in its polished initial state (top row) and after GD etching at different etching times (bottom row). Each column shows images captured at identical locations before and after GD etching. For both surface conditions, identical carbide grains on the surface are marked with red lines for easy identification. (For interpretation of the references to colour in this figure legend, the reader is referred to the web version of this article.)

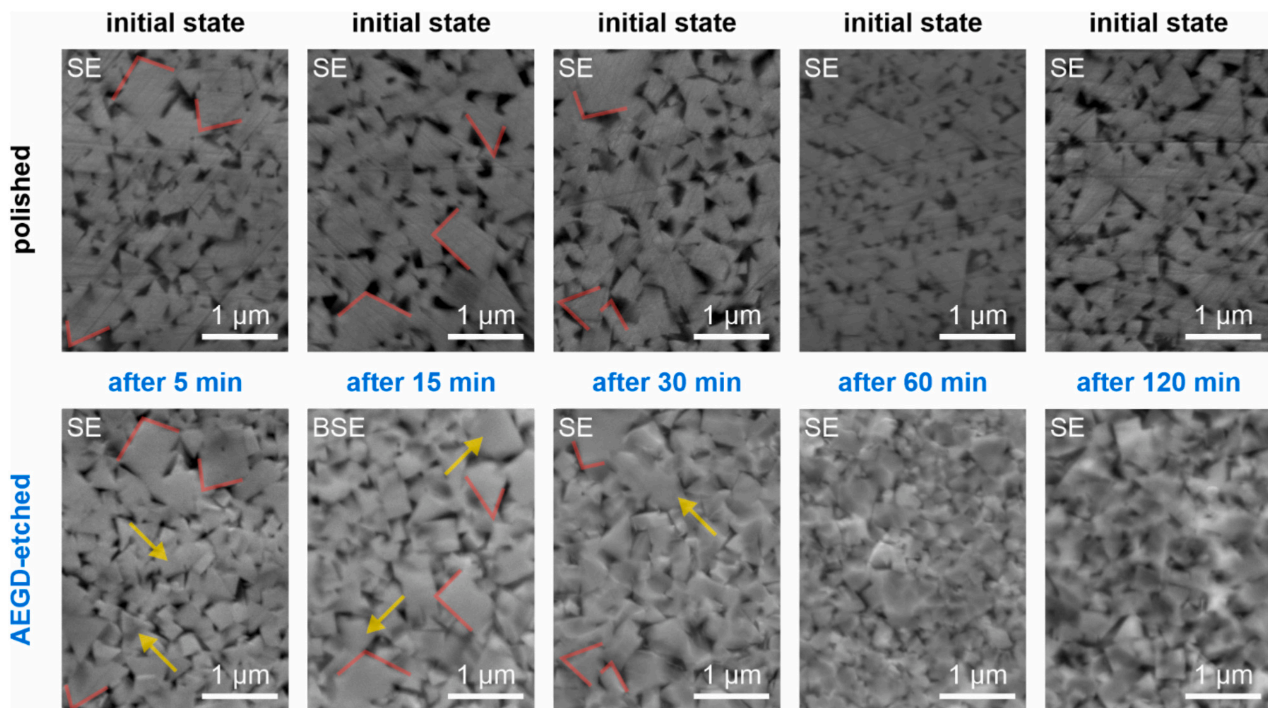

Fig. 5. SEM micrographs of the surface of the ultrafine-grained WC-Co cemented carbide in its polished initial state (top row) and after AEGD etching at different etching times (bottom row). Each column shows images captured at identical locations before and after AEGD etching. For both surface conditions, identical carbide grains on the surface are marked with red lines for easy identification. The yellow arrows indicate examples of carbides whose edges and corners have been rounded by AEGD etching. (For interpretation of the references to colour in this figure legend, the reader is referred to the web version of this article.)

as the resulting average cutting edge rounding $\bar{S}$ and the form-factor K [39]. Fig. 3 shows a schematic representation of the form-factor method to illustrate these parameters. The measurements of the cutting edge as well as the profile extractions were performed on a focus variation microscope EdgeMaster (Alicona Imaging GmbH, Austria).

The cutting tests were conducted using a three-axis machine tool

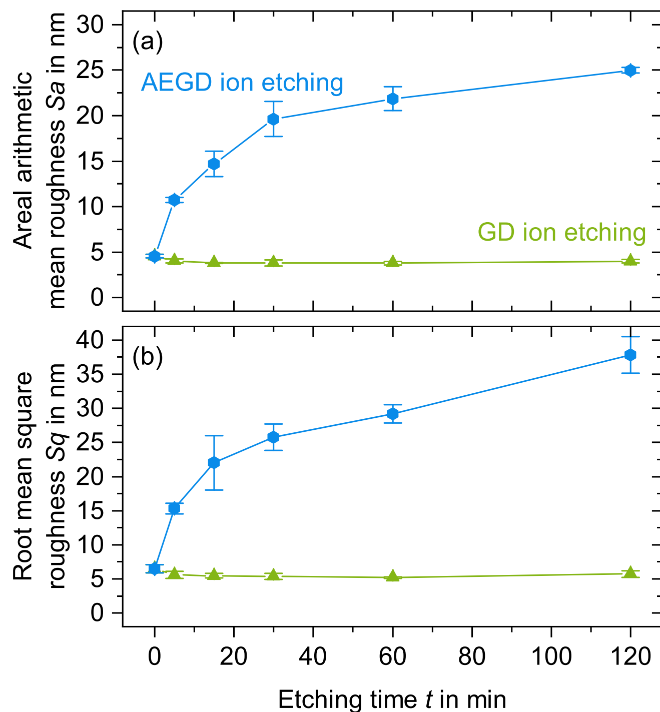

Fig. 6. (a) Areal arithmetic mean roughness *Sa* and (b) root mean square roughness *Sq* of GD- and AEGD-etched ultrafine-grained WC-Co cemented carbide.

HSPC 2522 (Kern Microtechnik GmbH, Germany). The operational behavior of the tools was evaluated in a down milling process over a maximum tool travel path of $l = 7.7$ m. The micromilling processes were carried out in dry condition with a cutting depth of $a_p = 25$ μm, a width of cut $a_e = 200$ μm, a feed per tooth $f_z = 25$ μm, and a cutting speed $v_c = 120$ m/min. A hardened and tempered powder metallurgical high-speed steel AISI M3:2, with a hardness of (62 ± 1) HRC served as workpiece material. The process forces were measured using a piezoelectric multicomponent dynamometer MicroDyn 9109 AA (Kistler Instrumente AG, Switzerland) with a sampling rate of 100 kHz. The wear behavior of the micro end mills was evaluated by measuring the width of the flank wear land *VB* using a digital microscope VHX-5000 (Keyence Corporation, Japan).

3. Results and discussion

3.1. Topography, roughness, and etch rates of GD- and AEGD-etched WC-Co cemented carbides

The surface of the ultrafine-grained WC-Co cemented carbide was analyzed by SEM in its polished initial state and after the ion etching process. Fig. 4 and Fig. 5 show SEM micrographs of the polished surface and the surfaces after GD or AEGD etching, respectively. These images were consistently captured from identical points on the surface before (top row) and after ion etching (bottom row) at different etching times, allowing to evaluate topographical changes resulting from ion etching over varying etching times. It is important to note that each column represents a distinct location on the surface. In the initial state, no smeared Co layer is identified on the surface, which is typically caused by grinding during the mechanical preparation of the WC-Co cemented carbide substrates. Since the substrates were polished in the final step, it is expected that the smeared Co layer was effectively removed from the surface. For the GD-etched WC-Co substrates, no significant topographical changes are observed, even with extended etching times. In this regard, identical carbide grains are discernible in the same locations

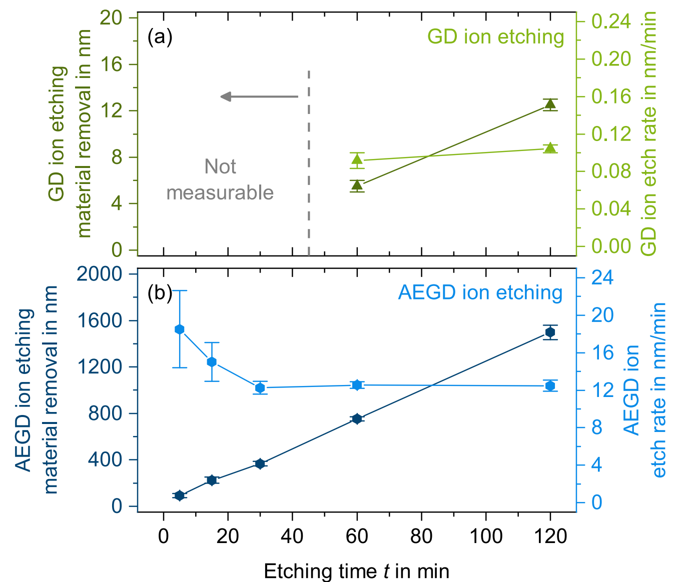

Fig. 7. (a) Material removal and (b) corresponding etch rates for GD and AEGD ion etching of ultrafine-grained WC-Co cemented carbide. The substrates were set in two-fold rotation.

on the surface before and after GD ion etching. This is clearly seen in Fig. 4, where exemplary grains have been highlighted with red lines along their corners and edges for easy identification.

The areal arithmetical mean roughness *Sa* and root mean square roughness *Sq* of the GD-etched ultrafine-grained WC-Co are depicted in Fig. 6. In the as-polished state, the WC-Co substrate exhibits a *Sa* value of (4.6 ± 0.2) nm and a *Sq* value of (6.5 ± 0.6) nm (depicted as 0 min in Fig. 6). The GD-etched WC-Co cemented carbide reveals a slightly lower roughness at a comparable level, with *Sa* ranging from 3.8 to 4.0 nm and *Sq* ranging from 5.2 to 6.5 nm, regardless of the etching time. This minor decrease in roughness is presumed to result from an initially stronger etching of the roughness asperities and a rounding of the corners and edges of the WC grains, although it is not clearly visible in the SEM images due to the small size of the carbide grains.

Fig. 5 presents SEM micrographs of both the polished and AEGD-etched ultrafine-grained WC-Co cemented carbides. The scratches generated on the surface during metallographic preparation were initially clearly visible but were completely eradicated after just 5 min of AEGD ion etching. Evidently, the intense Ar^+ ion bombardment in AEGD ion etching results in substantial material removal, effectively smoothing out the scratches. Gassner et al. also observed a reduction in the density and depth of scratches with increasing etching duration in their employed ion etching process [26]. It can be clearly seen that the topography of the WC-Co cemented carbide substrate undergoes significant changes with extended AEGD etching times. The edges and corners of the AEGD-etched WC grains become rounded, leading to an enlargement of the spaces where the Co binder is located. This is indicated by yellow arrows for exemplarily chosen carbide grains in Fig. 5. Identical carbide grains persist in the same locations on the surface even after AEGD ion etching with etching times of up to 30 min. In Fig. 5, corners and edges of exemplary chosen grains are delineated with red lines for both surface conditions. However, as etching time increases, locating the same tungsten carbides becomes progressively challenging, and at 60 and 120 min of etching time, the carbide distribution on the surface deviates entirely from the initial state. This suggests that prolonged AEGD etching times result in the complete removal of carbide grains from the surface. These topographical changes manifest in the surface roughness of the AEGD-etched substrates (see Fig. 6). The roughness values *Sa* and *Sq* progressively increase with longer etching times, rising from *Sa* = (10.7 ± 0.3) nm and *Sq* = (15.3 ± 0.8) nm after

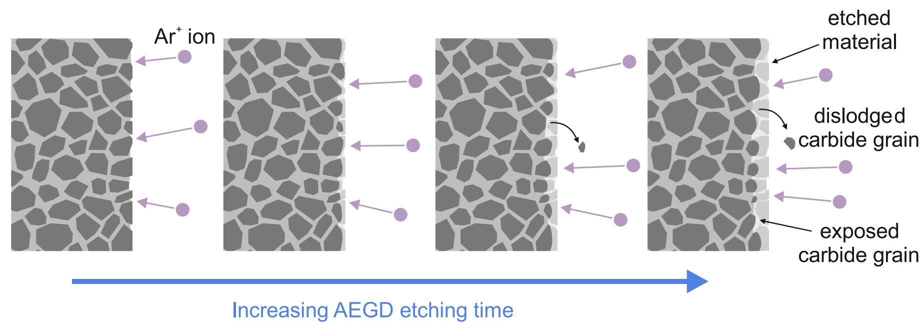

Fig. 8. Schematic illustration of the AEGD ion etching for ultrafine-grained WC-Co cemented carbide

5 min to $Sa = (25.0 \pm 0.3)$ nm and $Sq = (37.9 \pm 2.7)$ nm after 120 min of AEGD ion etching. An augmented roughness due to etching is advantageous, as it enhances the mechanical bonding between the substrate and a subsequently deposited PVD thin film, ensuring a higher adhesive strength [40]. Gassner et al. reported an initial roughness of $Sa \approx 8$ nm for fine-grained WC-Co cemented carbide in the polished state, which increased to $Sa \approx 31$ nm after 80 min of ion etching using their unspecified ion etching technique [26]. The AEGD-etched ultrafine-grained WC-Co cemented carbide displays a similar increase in roughness as the etching time extended from 0 to 120 min. However, a direct comparison between the roughness values is cautioned due to the distinct etching processes and carbide types employed. Thus, the emphasis is on illustrating the trend of increasing roughness with prolonged etching time.

Fig. 7(a) shows the material removal through GD ion etching and the calculated etch rate in relation to the etching time for substrates with two-fold rotation. Within the initial 5, 15, and 30 min, the material removal could not be distinctly determined, as it was within the same order of magnitude as the surface roughness. However, with longer etching durations, the material removal became discernible. It increases approximately linearly from (5.5 ± 0.5) nm after 60 min to (12.5 ± 0.5) nm after 120 min. The etch rate remains relatively constant at a low level of approximately 0.1 nm/min, regardless of the etching time. Thus, it can be anticipated that GD ion etching with etching times between 60 and 120 min will exhibit a linear trend in material removal. For comparison, the ultrafine-grained WC-Co cemented carbide was subjected to GD ion etching using another industrial PVD device. Similar parameters, including a bias voltage of $U_b = -650$ V, were employed for 60 min. The material removal is relatively low with (16.3 ± 2.4) nm, resulting in an etch rate of (0.27 ± 0.04) nm/min, which aligns with the obtained values.

The material removal and corresponding etch rates of AEGD ion etching are illustrated in Fig. 7(b). The material removal increases from (93 ± 18) nm after 5 min to (1498 ± 63) nm after 120 min of AEGD ion etching. Excluding the values for 5 and 15 min of AEGD ion etching time, the calculated etch rate ranges between (12.3 ± 0.7) and (12.5 ± 0.3) nm/min. The etch rate is significantly higher at 5 and 15 min with (18.5 ± 4.1) and (15.0 ± 2.1) nm/min, respectively. One explanation for this discrepancy is the ramping time of 11 min required to reach the desired bias voltage and currents, during which material removal may already occur. As the material removal during ramping constitutes a significant portion of the total material removal at low etching times of 5 or 15 min, this results in an overestimation of the etch rate at these durations. Apart from that, the higher etch rates for short etching durations can also be attributed to the initial greater etching removal of the Co binder over the WC grains.

In addition, the material removal was also exemplarily analyzed on the shaft of the micro end mills with three-fold rotation at an etching time of 120 min. At this etching duration, etching depths of (36 ± 12) nm for GD ion etching and (2132 ± 164) nm for AEGD ion etching were determined. This corresponds to etch rates of (0.3 ± 0.1) nm/min for GD ion etching and (17.8 ± 1.4) nm/min for AEGD ion etching. The values obtained for three-fold rotation are higher compared to those for two-fold rotation and are attributed to continuous ion bombardment from all directions. The etch rates are expected to remain constant for long etching durations, as observed for two-fold rotation. Given the initial diameter of $D = 1$ mm of the micro end mills and the material removal observed, the diameter is estimated to be reduced to approximately $D \approx 0.996$ mm after AEGD ion etching for 120 min. This small change in diameter is not expected to have a detrimental effect on the cutting behavior.

In general, the etch rate correlates with the sputtering yield, which describes the number of ejected substrate atoms per incident Ar^+ ion. The sputtering yield depends on the surface binding energy of the substrate material and the energy of the argon ions, which in turn is influenced by the bias voltage [18]. As the bias voltage is kept constant at $U_b = -300$ V for GD ion etching and $U_b = -650$ V for AEGD ion etching, while varying the etching time and keeping the substrate material unchanged, the sputtering yield and, consequently, the etch rate remains nearly constant for both GD and AEGD ion etching. The negative bias voltage applied to the substrate holder attracts Ar^+ ions towards the substrate's surface. Consequently, increasing the bias voltage accelerates the Ar^+ ions with higher kinetic energy, typically resulting in a higher etch rate. This is because the sputtering yield of a single Ar^+ ion is significantly influenced by both its mass and kinetic energy. However, despite the higher bias voltage of $U_b = -650$ V for GD ion etching, the resulting etch rates are approximately 100 times lower than those obtained by AEGD ion etching at a bias voltage of $U_b = -300$ V. Therefore, the significantly higher etch rates in AEGD ion etching are attributed to the elevated ionization degree of the process gas Ar and, consequently, a higher flux of impinging Ar^+ ions on the substrate's surface. For fine-grained WC-Co cemented carbides, Gassner et al. reported an etch rate of (8 ± 1) nm/min for their unspecified ion etching process at a bias voltage of $U_b = -185$ V [26]. This value is significantly higher than that achieved with conventional GD ion etching but falls below the etch rates obtained with AEGD ion etching under the employed parameters. This difference may be attributed to variations in the type of WC-Co cemented carbide or the ion etching process itself.

The material removal during prolonged AEGD ion etching significantly surpasses the grain size of the ultrafine-grained WC-Co cemented carbide. Consequently, the intensive bombardment with Ar^+ ions is expected not only to etch the Co binder and WC carbides but also to potentially remove carbides from the Co matrix. Fig. 8 illustrates a scheme of the mechanisms of material removal for ultrafine-grained WC-Co cemented carbide in dependency of the AEGD ion etching time. Initially, the Co binder is more profoundly etched due to its higher sputtering rate resulting in more exposed WC grains. As the etching progresses, both the Co binder and WC carbides undergo further etching removal, leading to a substantial rounding of edges and corners of the WC grains. If the mechanical bonding of the Co binder is able to retain the WC carbides, the WC grains are completely removed by etching until the underlying carbides are exposed. However, it is essential to consider

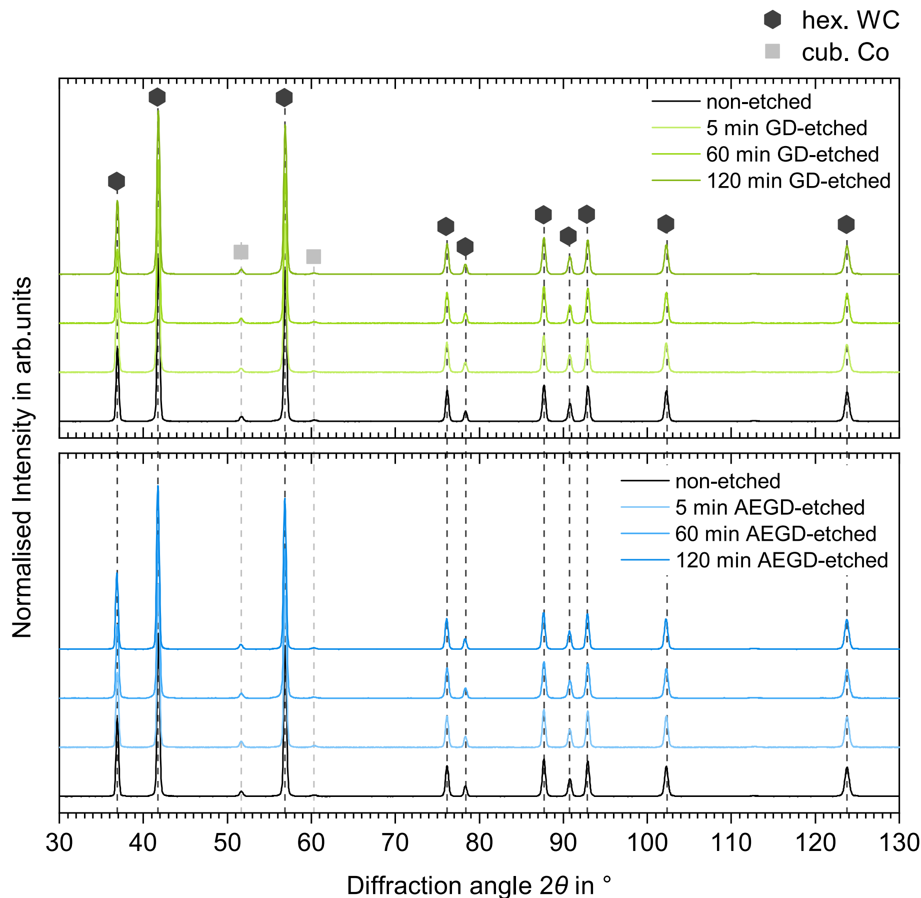

Fig. 9. X-ray diffractograms obtained of GD- and AEGD-etched ultrafine-grained WC-Co cemented carbide.

that intensive etching of the Co binder may weaken the mechanical bonding, resulting in the release of carbides and the exposure of underlying carbides. Dislodged carbides contribute significantly to an increase in roughness, as the resulting gaps form valleys on the surface. Despite the extensive material removal, no cross-contamination effect was observed on the surface of the etched WC-Co cemented carbide. It is important to note that the surface area of the substrates and the micro end cutters were positioned vertically. However, an accumulation of detached carbides may occur on parts with open, curved surfaces and should be carefully considered.

3.2. *Phase composition and stress state of GD- and AEGD-etched WC-CO cemented carbides*

The phase analysis was performed by XRD to evaluate possible crystallographic changes caused by the ion etching processes. The diffractograms of the non-etched, GD-etched, and AEGD-etched ultrafine-grained WC-Co cemented carbide are depicted in Fig. 9. For a better overview, only the etched substrates with etching times of 5, 60, and 120 min are shown. The Bragg reflections located at 36.9°, 41.8°, 56.9°, 76.2°, 78.4°, 87.7°, 90.7°, 92.8°, 102.4°, and 123.8° correspond to the hexagonal WC phase (space group $P\overline{6}m2$), whereas the diffraction angles located at 51.7° and 60.3° originate from the face-centered cubic (fcc) α-Co phase (space group $Fm\overline{3}m$). The diffraction angles of Co show a low intensity due to the low Co content in the ultrafine-grained WC-Co cemented carbide. The differently etched WC-Co substrates demonstrate an identical diffraction pattern to the non-etched state, characterized by identical Bragg reflections with comparable intensities. It can be concluded that the etching pretreatments performed did not induce high heat flux leading to significant crystallographic changes, such as thermal

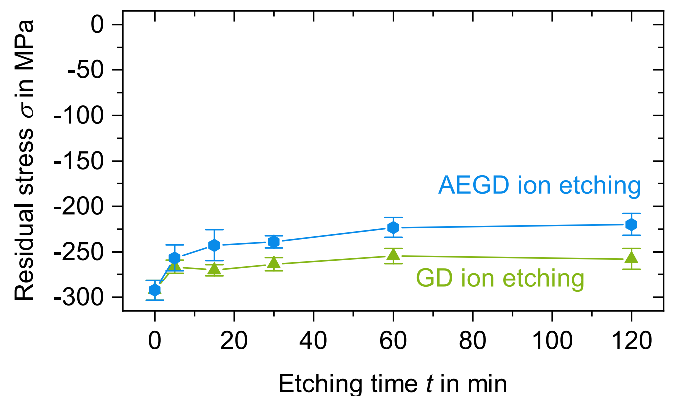

Fig. 10. Residual stress of GD- and AEGD-etched ultrafine-grained WC-Co cemented carbide.

decomposition of WC to the W_2C phase. However, it should be noted that the maximum penetration depth for Co Kα radiation is about z_0 = 1.3 μm in WC and about z_0 = 7.9 μm in Co [37]. Hence, the considered phase composition corresponds to this edge area of the WC-Co substrates. For metal-ion-etched steel surfaces, modified edge zones with a depth of 5 nm were determined [41]. Therefore, if structural changes occurred in the surface edge zone due to GD and AEGD ion etching, these are of low degree and only in the nm range, making them undetectable by XRD.

In addition, the residual stresses of the ultrafine-grained WC-Co cemented carbide were calculated from the strains using the elastic constants for the (112) plane of WC located at around 124° (see Fig. 10).

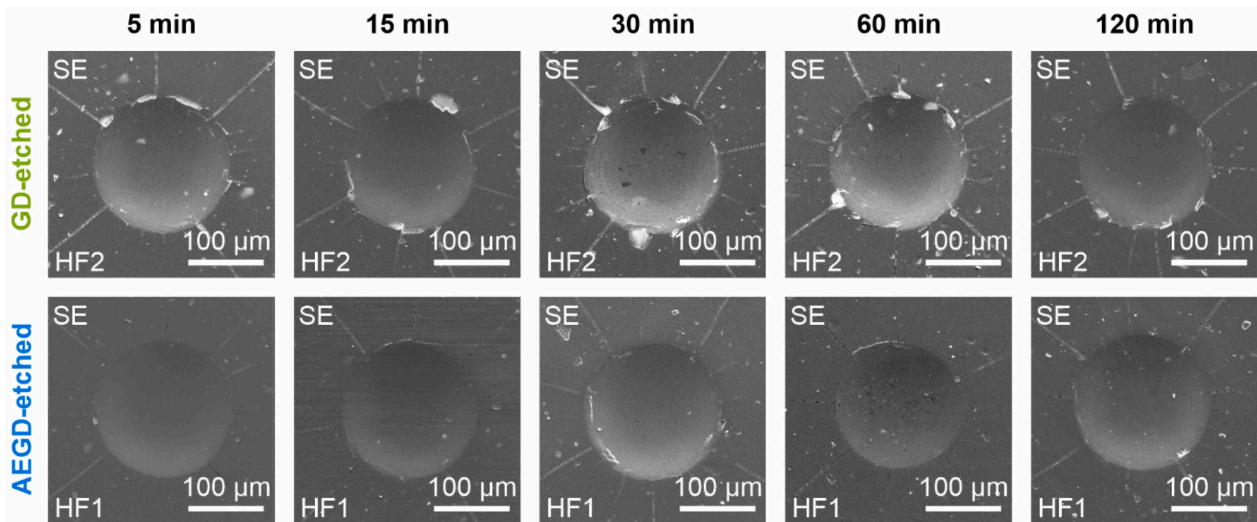

Fig. 11. SEM micrographs of the Rockwell C indents performed on the HiPIMS-TiAlSIN coated on the GD- and AEGD-etched ultrafine-grained WC-Co cemented carbide

In the as-delivered grounded state, the WC-Co substrate exhibits high compressive stress of $\sigma = -(1400 \pm 30)$ MPa. The grinding process generally induces significant compressive stresses in the near-surface region due to high mechanical loads, while thermal loads are suppressed by the coolant [42]. After the metallographic preparation, the WC-Co substrate reveals a lower compressive stress of $\sigma = -(290 \pm 10)$ MPa (depicted as 0 min in Fig. 10). Specifically, the polishing step removes material through soft abrasion without causing deformation-induced compressive stresses, thereby exposing the subsurface area with lower degree of deformation state [43].

Both the GD- and AEGD-etched WC-Co substrates exhibit slightly reduced compressive stresses. A decrease in compressive stresses is commonly observed for WC-CO cemented carbides after the heating and ion etching sequence [42]. In addition to the initial heating sequence in the PVD process, the ion etching procedure has a thermal effect due to the intensive ion bombardment, leading to stress relief. A significant reduction in residual stress is observed, especially in grounded WC-Co with high residual compressive stresses, while polished WC-Co with very low residual compressive stresses exhibits moderate changes in the stress state [44]. The compressive stresses of the GD-etched WC-Co cemented carbides remain at a comparable level, ranging from −260 to −270 MPa, regardless of the etching time. In this case, it is expected that the heating predominantly influences the thermal effect rather than GD ion etching. In contrast, the compressive stresses slightly decrease from $\sigma = -(270 \pm 10)$ to $\sigma = -(220 \pm 10)$ MPa with increasing etching time from 5 to 120 min for the AEGD-etched WC-Co substrates. On the one hand, the intensive AEGD ion etching with a high flux of impinging Ar^+ ions generates sufficient heat into the surface edge zone to further reduce the residual stresses, as the measured substrate temperature of $T = 350$ °C is higher compared to GD ion etching with $T = 320$ °C. On the other hand, the Co binder is removed at a faster etch rate than the WC grains, resulting in a relief of compressive stresses [45]. With longer AEGD ion etching durations leading to increased material removal, a greater reduction in compressive stresses can be anticipated. However, it is important to note that the WC-Co cemented carbide exhibits a stress gradient with a baseline of compressive stresses within a depth over several µm [43]. In this regard, the substantial material removal in AEGD ion etching may also expose a zone with reduced compressive stresses.

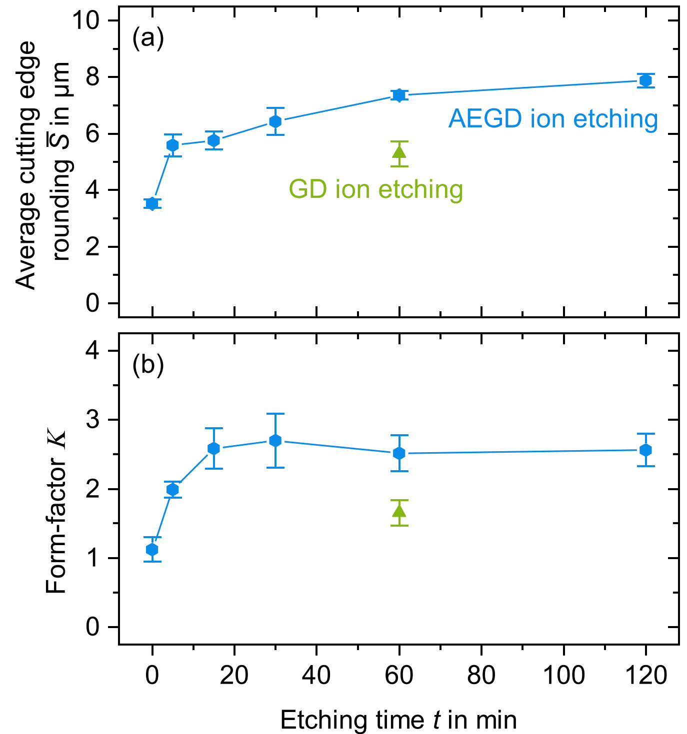

Fig. 12. (a) Average cutting edge rounding $\bar{S}$ and (b) form-factor K of the GD- and AEGD-etched micro end mills coated with HiPIMS-TiAlSiN (data taken from [30]).

3.3. Adhesion of HiPIMS-TiAlSiN on GD- and AEGD-etched WC-Co cemented carbides

The adhesion of the HiPIMS-TiAlSiN thin film on the GD- and AEGD-etched ultrafine-grained WC-Co cemented carbide was evaluated through Rockwell C indentation test. Fig. 11 shows SEM micrographs of the Rockwell indents generated on the substrates for varying etching durations. The HiPIMS-TiAlSiN thin film exhibits minor spalling failures around the indent edge for GD-etched WC-Co cemented carbide with etching times ranging from 5 to 120 min. Consistent with this failure pattern across different etching times, an adhesion class 2 is assigned to

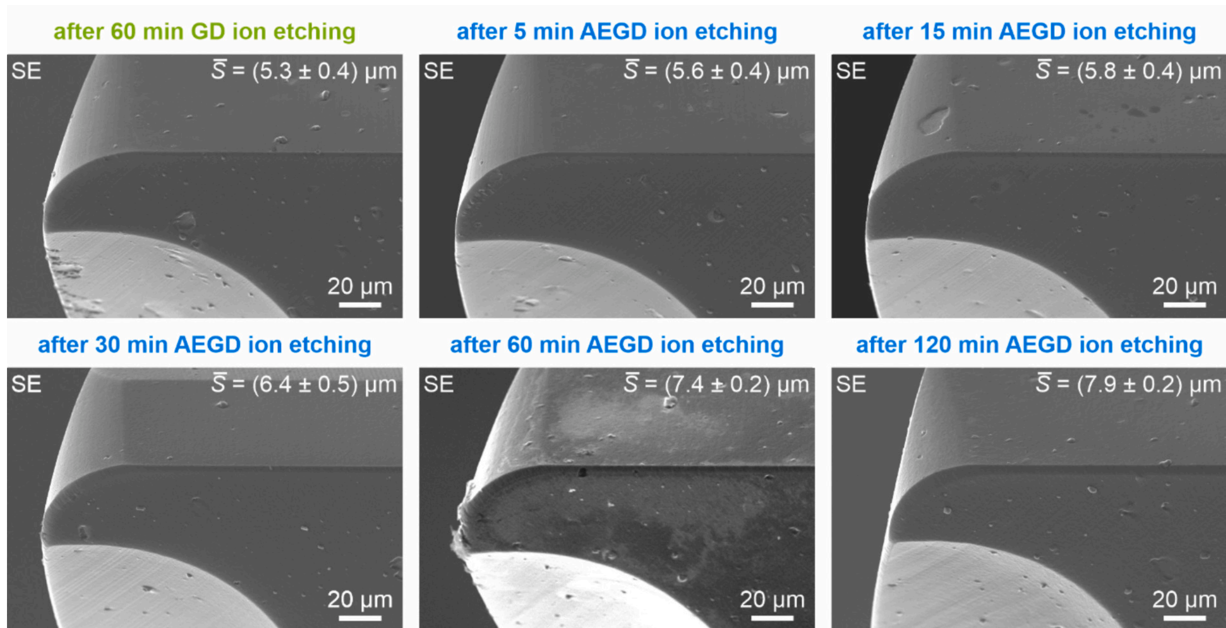

Fig. 13. SEM micrographs of the cutting corner of the GD- and AEGD-etched micro end mills coated with HiPIMS-TiAlSiN.

the HiPIMS-TiAlSiN thin film on all GD-etched substrates. In contrast, already 5 min AEGD ion etching is sufficient to ensure high thin film adhesion without any delamination failure. As a result, the adhesion of the HiPIMS-TiAlSiN thin film on all AEGD-etched substrates is categorized into the highest adhesion class 1. With longer AEGD etching times of up to 120 min, the HiPIMS-TiAlSiN thin film on the WC-Co cemented carbide continues to exhibit high adhesion classified as HF1. The improved thin film adhesion on AEGD-etched ultrafine-grained WC-Co cemented carbide is attributed to improved chemical bonding, resulting from the removal of impurities and oxides from the substrate surface during AEGD ion etching. Additionally, the increase in surface roughness contributes to improved mechanical bonding between the thin film and the substrate.

3.4. *Cutting edge geometry and cutting performance of GD- and AEGD-etched WC-Co micro end mills*

For cutting tools, it is essential to consider the impact of the high material removal during AEGD ion etching on the cutting edge geometry. In a previous study, the authors demonstrated that AEGD ion etching leads to substantial changes to the cutting edge geometry of micro end mills [30]. Fig. 12 shows the average cutting edge rounding $\overline{S}$ and form-factor K of the AEGD-etched tools with subsequent HiPIMS-TiAlSiN deposition. For comparison, GD ion etching for 60 min was also applied to assess its effect on the cutting edge geometry. SEM micrographs of the cutting corners of the micro end mills are presented in Fig. 13. In the initial state without ion etching and HIPIMS-TiAlN thin film (depicted as 0 min), the micro end mill exhibits an average cutting edge rounding of $\overline{S} = (3.5 \pm 0.2)$ µm and a form-factor of $K \approx 1.1$. After the deposition of a PVD thin film, the cutting edge usually possesses an increase in cutting edge rounding. However, in this case, the AEGD ion etching leads to a significant augmentation of the average cutting edge rounding. This effect is particularly noticeable with increasing etching time, as the rise in cutting edge rounding steadily rises from $\overline{S} \approx 5.6$ µm for 5 min to $\overline{S} \approx 7.9$ µm for 120 min. The increased cutting edge rounding can be clearly seen in the respective SEM micrographs. A direct comparison between both ion etching methods also highlights the substantial impact of AEGD ion etching on the cutting edge, as the tools exhibit a larger rounding with $\overline{S} = (7.4 \pm 0.2)$ µm after 60 min of AEGD ion etching compared to the GD-etched ones with $\overline{S} = (5.3 \pm 0.4)$ µm for the same etching time. In addition to the increased cutting edge rounding, AEGD ion etching also results in stronger asymmetry of the cutting edge geometry. AEGD ion etching for 5 min yields $K \approx 2.0$, and longer etching times lead to significantly higher K values ranging from 2.5 to 2.7. A plateau in the form-factor seems to emerge at extended etching times. Form-factors exceeding $K > 1.0$ are indicative of an asymmetrical cutting edge rounding [39].

When interpreting the previous obtained results in the context of the achieved etch rates, it becomes evident that substantial material removal plays a decisive role in the cutting edge rounding. The asymmetrical cutting edge results from more pronounced rounding and correspondingly greater material removal on the rake face. Achieving such edge rounding with the very low etch rates of GD ion etching would be improbable. This effect of the AEGD ion etching can be attributed, on the one hand, to the anodically poled arc evaporators, which attract electrons from the AEGD module towards the substrate carousel, thereby enhancing ionization of the argon gas. The tools are positioned in the holder systems so that the lateral surface of the tools aligns with the trajectory of the electrons, potentially exposing the rake face to a higher plasma density. On the other hand, the pulsed bias voltage also influences the formation of a glow seam on edges and corners of the tools. In combination with the high ionization degree of AEGD, this may also lead to higher plasma densities on the cutting edge.

In the realm of conventional machining, the beneficial effects of asymmetrical cutting edge shapes ($K > 1$) have already been sufficiently investigated [39,46]. Unfavorable influences of a cutting edge preparation can be avoided by inclining the microgeometry. In particular, workpiece side material flows, the resulting rise in passive forces, and the associated mechanical tool load can be limited by reducing the free surface preparation [39,46]. Until now, however, it has only been possible to transfer these findings to micromachining to a limited extent due to the manufacturability of asymmetrical cutting edge geometries in very small sizes. Therefore, AEGD ion etching with its high material removal emerges as a promising method for creating asymmetrical cutting edge geometries on filigree milling tools. A prior study demonstrated that such AEGD-etched tool geometries, when applied to micro end cutters coated with HiPIMS-TiAlSiN, effectively minimize wear and process forces during the dry machining of hardened and tempered powder metallurgical high-speed steel AISI M3:2 with a hardness of (62 ± 1) HRC [30]. These findings demonstrate the positive impact of

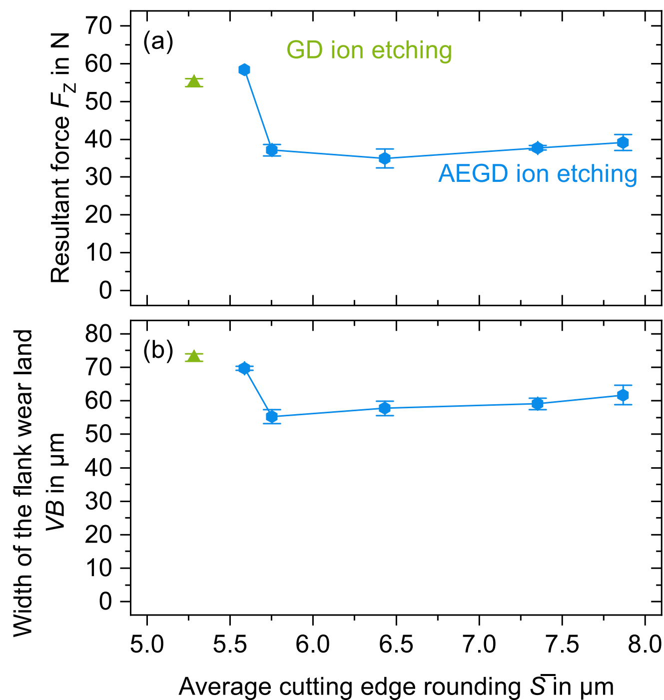

Fig. 14. (a) Cutting force F_Z and (b) width of the flank wear land *VB* of the GD- and AEGD-etched micro end mills coated with HiPIMS-TiAlSiN after reaching the maximum milling path in micromilling a hardened and tempered powder metallurgical high-speed steel AISI M3:2 (data taken from [30]).

asymmetrical cutting edge geometries in micro-scale machining. This is particularly important given the increased material flows on the workpiece side due to ploughing in micromachining [47] and reveals the great potential as well as the necessity of cutting edge shapes adapted to micro-hard machining process.

In the machining tests, the operational performance and wear behavior of the micro end mills were analyzed in micromilling high-speed steel AISI M3:2. Fig. 14 shows the resultant force F_Z and the width of the flank wear land *VB* of the cutting tools upon reaching the maximum considered travel path of $l = 7.7$ m, plotted against the average cutting edge rounding $\bar{S}$. SEM micrographs of the corresponding worn cutting corners of the GD- and AEGD-etched micro end mills are presented in Fig. 15. All cutting corners experienced abrasive wear along the flank face. The resultant force and tool wear behavior are notably influenced by the set etching time, respectively the achieved cutting edge geometry. Micro end mills with minimal cutting edge rounding $\bar{S}$, which were pretreated with GD ion etching for 60 min and AEGD ion etching for 5 min, exhibit high resultant forces F_Z in the ranging from 55 to 59 N and high width of the flank wear land *VB* ranging from 70 to 72 µm. However, increasing the cutting edge rounding by AEGD ion etching with durations $t \geq 15$ min achieves a reduction of the resultant force and tool wear. In this regard, micro end mills with cutting edge roundings of $\bar{S} = (5.8 \pm 0.3)$ µm and $\bar{S} = (6.4 \pm 0.5)$ µm, which resulted from 15 and 30 min AEGD ion etching, reach the lowest resulting resultant force of $F_Z = (35 \pm 3)$ N as well as width of the flank wear land of $VB = (55 \pm 2)$ µm. Prolonged AEGD ion etching times lead to a slight increase in resultant forces and tool wear. Extensive AEGD ion etching and, consequently, more intensified cutting edge preparation result in increased mechanical loads, leading to higher resultant forces and wear. Therefore, AEGD ion etching with shorter etching times of 15 and 30 min forms advantageous cutting edge geometries, promoting improved cutting performance in the considered micromilling process of high-speed steel.

4. Conclusions

AEGD ion etching of ultrafine-grained WC-Co cemented carbide exhibits significant material removal at high etch rates ranging from 12 to 13 nm/min during extended etching times. In contrast to conventional GD ion etching, AEGD ion etching achieves a 100-fold increase in etch rate, surpassing the order of the WC grain size at elevated etching durations. This suggests that the carbides are not only entirely etched but may also become dislodged from the Co binder if the mechanical interlocking is weakened due to the severe removal of the binder matrix. While GD-etched WC-Co substrates show comparable a comparable

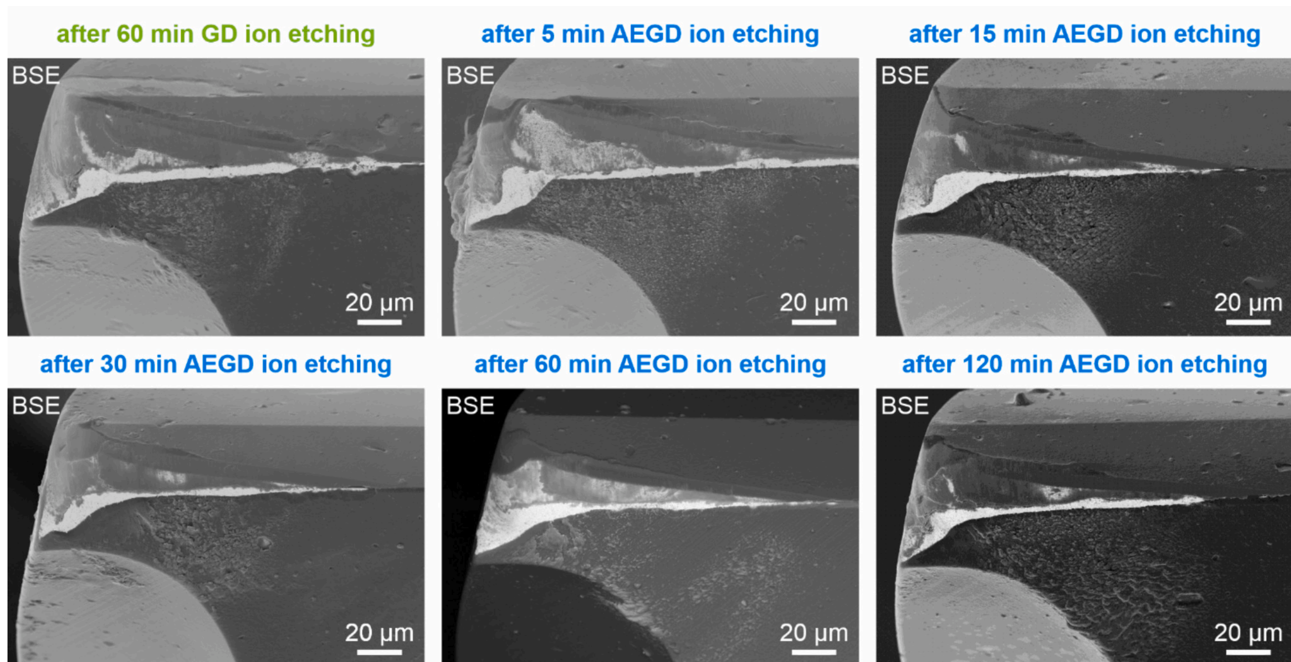

Fig. 15. SEM micrographs of the worn cutting corner of the GD- and AEGD-etched micro end mills coated with HiPIMS-TiAlSiN after micromilling a hardened and tempered powder metallurgical high-speed steel AISI M3:2.

surface roughness with Sa value ranging from 3.8 to 4.0 nm, the surface roughness of AEGD-etched WC-Co steadily increases from $Sa = (10.7 \pm 0.3)$ nm after 5 min to $Sa = (25.0 \pm 0.3)$ nm after 120 min. The crystalline phase composition of WC-Co remains unaffected by the etching processes, but the compressive stresses within the WC grains are slightly reduced due to the heating sequence and etching procedure. In this context, AEGD ion etching contributes to a gradual decrease in compressive stresses with increasing etching time, attributed to the thermal input resulting from intensive ion bombardment. In comparison to GD ion etching, AEGD ion etching promotes higher adhesion of the HiPIMS-TiAlSiN thin film on ultrafine-grained WC-Co cemented carbide. The intense material removal not only removes contamination and oxide layers from the surface but also leads to a rougher surface. This enhances both chemical and mechanical bonding between the thin film and substrate material, significantly improving adhesion strength. Furthermore, this higher material removal leads to a certain effect on the cutting edge geometry. The intensive AEGD ion etching not only increases the average cutting edge rounding from $\overline{S} \approx 5.6$ µm for 5 min to $\overline{S} \approx 7.9$ µm for 120 min but also produces an asymmetrical cutting edge geometry with form-factors $K \geq 2$ in the given process configuration. In micromilling high-speed steel, these cutting edge geometries have proven to be beneficial in effectively reducing cutting forces and wear over the considered travel path of $l = 7.7$ m. Especially cutting edge roundings $\overline{S}$ in the range between 5.6 and 6.5 µm achieved the lowest process forces as well as widths of the flank wear land. Consequently, AEGD ion etching emerges as a promising method for improving thin film adhesion and, with respect to filigree precision cutting tools, for preparing asymmetrical cutting edge geometries to enhance cutting performance and wear resistance.

CRediT authorship contribution statement

Nelson Filipe Lopes Dias: Writing – original draft, Visualization, Project administration, Investigation, Formal analysis, Data curation, Conceptualization. **Alexander Leonard Meijer:** Writing – original draft, Visualization, Project administration, Investigation, Formal analysis, Data curation, Conceptualization. **Christoph Paul Jäckel:** Investigation. **Alexander Frisch:** Visualization, Investigation. **Dirk Biermann:** Writing – review & editing, Supervision, Resources, Funding acquisition. **Wolfgang Tillmann:** Writing – review & editing, Supervision, Resources, Funding acquisition.

Declaration of generative AI and AI-assisted technologies in the writing process

During the preparation of this work, the authors used ChatGPT and DeepL in order to improve language and readability. After using these tools, the authors reviewed and edited the content as needed and take full responsibility for the content of the publication.

Declaration of competing interest

The authors declare that they have no known competing financial interests or personal relationships that could have appeared to influence the work reported in this paper.

Data availability

Data will be made available on request.

Acknowledgements

The authors gratefully acknowledge the financial support of the Deutsche Forschungsgemeinschaft (DFG, German Research Foundation, Germany) within the project 445127534 (TI 343/187-1, BI 498/126-1). The authors would also like to thank Dr. Dominic Stangier and Dr. Jürgen Müller of Oerlikon Balzers Coating Germany GmbH for their consultation and support in designing the AEGD etching process.

References

[1] F. Klocke, Manufacturing Processes 1: Cutting, Springer, Berlin / Heidelberg, Berlin, Heidelberg, 2011.
[2] E. Krebs, M. Wolf, D. Biermann, W. Tillmann, D. Stangier, High-quality cutting edge preparation of micromilling tools using wet abrasive jet machining process, Prod. Eng. Res. Devel. 12 (2018) 45–51, https://doi.org/10.1007/s11740-017-0787-7.
[3] E. Uhlmann, D. Oberschmidt, Y. Kuche, A. Löwenstein, Cutting edge preparation of micro milling tools, Procedia CIRP 14 (2014) 349–354, https://doi.org/10.1016/j.procir.2014.03.083.
[4] E. Uhlmann, D. Oberschmidt, Y. Kuche, A. Löwenstein, I. Winker, Effects of different cutting edge preparation methods on micro milling performance, Procedia CIRP 46 (2016) 352–355, https://doi.org/10.1016/j.procir.2016.04.004.
[5] A. Meijer, D. Biermann, Machining of molds with filigree structures for sheet-bulk metal forming, in: M. Merklein, A.E. Tekkaya, B.-A. Behrens (Eds.), Sheet Bulk Metal Forming, Springer International Publishing, Cham, 2021, pp. 147–171.
[6] A.L. Meijer, D. Stangier, W. Tillmann, D. Biermann, Induction of residual compressive stresses in the sub-surface by the adjustment of the micromilling process and the tool's cutting edge, CIRP Ann. 71 (2022) 97–100, https://doi.org/10.1016/j.cirp.2022.04.065.
[7] W. Tillmann, D. Stangier, A. Meijer, E. Krebs, A. Ott, T. Platt, N.F. Lopes Dias, L. Hagen, D. Biermann, Adapting the surface integrity of high-speed steel tools for sheet-bulk metal forming, JMMP 6 (2022) 37, https://doi.org/10.3390/jmmp6020037.
[8] T. Wild, T. Platt, D. Biermann, M. Merklein, Analysis of the influence of surface modifications on the fatigue behavior of hot work tool steel components, Materials (Basel) 14 (2021), https://doi.org/10.3390/ma14237324.
[9] Z. Liang, S. Li, T. Zhou, P. Gao, D. Zhang, X. Wang, Design and fabrication of a new micro ball-end mill with conical flank face, Int. J. Adv. Manuf. Technol. 97 (2018) 39–50, https://doi.org/10.1007/s00170-018-1924-y.
[10] J. García, V. Collado Ciprés, A. Blomqvist, B. Kaplan, Cemented carbide microstructures: a review, Int. J. Refract. Met. Hard Mater. 80 (2019) 40–68, https://doi.org/10.1016/j.ijrmhm.2018.12.004.
[11] N. Chen, H.N. Li, J. Wu, Z. Li, L. Li, G. Liu, N. He, Advances in micro milling: from tool fabrication to process outcomes, Int. J. Mach. Tools Manuf. 160 (2021) 103670, https://doi.org/10.1016/j.ijmachtools.2020.103670.
[12] S.N.B. Oliaei, Y. Karpat, J.P. Davim, A. Perveen, Micro tool design and fabrication: a review, J. Manuf. Process. 36 (2018) 496–519, https://doi.org/10.1016/j.jmapro.2018.10.038.
[13] K.-D. Bouzakis, G. Skordaris, S. Gerardis, G. Katirtzoglou, S. Makrimallakis, M. Pappa, S. Bolz, W. Koelker, The effect of substrate pretreatments and HPPMS-deposited adhesive interlayers' materials on the cutting performance of coated cemented carbide inserts, CIRP Ann. 59 (2010) 73–76, https://doi.org/10.1016/j.cirp.2010.03.065.
[14] Y. Deng, W. Chen, B. Li, C. Wang, T. Kuang, Y. Li, Physical vapor deposition technology for coated cutting tools: a review, Ceram. Int. 46 (2020) 18373–18390, https://doi.org/10.1016/j.ceramint.2020.04.168.
[15] R.F. Bunshah, Handbook of Hard Coatings: Deposition Technologies, Properties and Applications, Noyes Publications; William Andrew Publishing, Park Ridge, New Jersey, Norwich, New York, 2001.
[16] P. Panjan, A. Drnovšek, M. Čekada, M. Panjan, Contamination of substrate-coating Interface caused by ion etching, Coatings 12 (2022) 846, https://doi.org/10.3390/coatings12060846.
[17] K. Mallika, R. Komanduri, Diamond coatings on cemented tungsten carbide tools by low-pressure microwave CVD, Wear 224 (1999) 245–266, https://doi.org/10.1016/S0043-1648(98)00337-8.
[18] D.M. Mattox, Handbook of Physical Vapor Deposition (PVD) Processing, Elsevier, 2010.
[19] J. Faber, G. Hötzsch, C. Metzner, Sputter etching of steel substrates using DC and MF pulsed magnetron discharges, Vacuum 64 (2001) 55–63, https://doi.org/10.1016/S0042-207X(01)00375-X.
[20] P. Panjan, A. Drnovšek, P. Gselman, M. Čekada, M. Panjan, Review of growth defects in thin films prepared by PVD techniques, Coatings 10 (2020) 447, https://doi.org/10.3390/coatings10050447.
[21] P.J. Kelly, R. Hall, J. O'Brien, J.W. Bradley, P. Henderson, G. Roche, R.D. Arnell, Studies of mid-frequency pulsed dc biasing, J. Vac. Sci. Technol. A 19 (2001) 2856–2865, https://doi.org/10.1116/1.1410949.
[22] K.E. Cooke, J. Hamsphire, W. Southall, D.G. Teer, The industrial application of pulsed DC bias power supplies in closed field unbalanced magnetron sputter ion plating, Surf. Coat. Technol. 177-178 (2004) 789–794, https://doi.org/10.1016/j.surfcoat.2003.06.009.
[23] B. Peng, Y.X. Xu, J.W. Du, L. Chen, K.H. Kim, Q. Wang, Influence of preliminary metal-ion etching on the topography and mechanical behavior of TiAlN coatings on cemented carbides, Surf. Coat. Technol. 432 (2022) 128040, https://doi.org/10.1016/j.surfcoat.2021.128040.
[24] S.M. Alves, W. Albano, A.J. de Oliveira, Improvement of coating adhesion on cemented carbide tools by plasma etching, J. Braz. Soc. Mech. Sci. Eng. 39 (2017) 845–856, https://doi.org/10.1007/s40430-016-0545-3.
[25] A.L. Meijer, A. Ott, D. Stangier, W. Tillmann, D. Biermann, Modification of surface and sub-surface conditions of cemented carbide by pressurized air wet abrasive jet

machining for PVD coatings, Procedia CIRP 108 (2022) 372–377, https://doi.org/10.1016/j.procir.2022.04.073.
[26] M. Gassner, N. Schalk, B. Sartory, M. Pohler, C. Czettl, C. Mitterer, Influence of Ar ion etching on the surface topography of cemented carbide cutting inserts, Int. J. Refract. Met. Hard Mater. 69 (2017) 234–239, https://doi.org/10.1016/j.ijrmhm.2017.08.015.
[27] S. Krassnitzer, O. Gstoehl, D. Lendi, Method and Apparatus for Manufacturing Cleaned Substrates or Clean Substrates Which Are Further Processed: European Patent Specification, EP 2 158 977 B1, 2010.
[28] J. Vetter, W. Burgmer, A.J. Perry, Arc-enhanced glow discharge in vacuum arc machines, Surf. Coat. Technol. 59 (1993) 152–155, https://doi.org/10.1016/0257-8972(93)90074-X.
[29] J. Vetter, T. Wallendorf, Plasma diagnostics of arc-enhanced glow discharge, Surf. Coat. Technol. 76-77 (1995) 322–327, https://doi.org/10.1016/0257-8972(95)02554-5.
[30] C.P. Jäckel, A.L. Meijer, D. Stangier, N.F. Lopes Dias, W. Tillmann, D. Biermann, Cutting edge preparation of micro end mills by PVD-etching technology, Prod. Eng. 5 (2024) 108, https://doi.org/10.1007/s11740-023-01257-9.
[31] Boehlerit GmbH & Co.KG, Carbide Blanks and Semi-finished Products for Manufacturers of Precision Tools. https://www.boehlerit.com/fileadmin/user_upload/PDF/Hartmetallstaebe_Carbide_rods.pdf, 2024 (accessed 7 January 2024).
[32] W. Tillmann, L. Hagen, D. Stangier, M. Krabiell, P. Schröder, J. Tiller, C. Krumm, C. Sternemann, M. Paulus, M. Elbers, Influence of etching-pretreatment on nano-grained WC-Co surfaces and properties of PVD/HVOF duplex coatings, Surf. Coat. Technol. 374 (2019) 32–43, https://doi.org/10.1016/j.surfcoat.2019.05.054.
[33] W. Tillmann, N.F. Lopes Dias, D. Stangier, W. Maus-Friedrichs, R. Gustus, C. A. Thomann, H. Moldenhauer, J. Debus, Improved adhesion of a-C and a-C:H films with a CrC interlayer on 16MnCr5 by HiPIMS-pretreatment, Surf. Coat. Technol. 375 (2019) 877–887, https://doi.org/10.1016/j.surfcoat.2019.07.076.
[34] W. Tillmann, D. Grisales, D. Stangier, I. Ben Jebara, H. Kang, Influence of the etching processes on the adhesion of TiAlN coatings deposited by DCMS, HiPIMS and hybrid techniques on heat treated AISI H11, Surf. Coat. Technol. 378 (2019) 125075, https://doi.org/10.1016/j.surfcoat.2019.125075.
[35] German Institute for Standardisation Registered Association, Geometrical Product Specifications (GPS) - Surface Texture: Areal - Part 2: Terms, Definitions and Surface Texture Parameters (ISO 25178-2:2021); German Version EN ISO 25178-2:2022, 2023.
[36] German Institute for Standardisation Registered Association, Geometrical Product Specifications (GPS) - Surface texture: Areal - Part 3: Specification Operators (ISO 25178-3:2012); German Version EN ISO 25178-3:2012, 2012.
[37] B. Eigenmann, E. Macherauch, Röntgenographische Untersuchung von Spannungszuständen in Werkstoffen. Teil III. Fortsetzung von Matwiss. und Werkstofftechn. Heft 3/1995, S. 148–160 und Heft 4/1995, S. 199–216, Mater. Werkst. 27 (1996) 426–437, https://doi.org/10.1002/mawe.19960270907.
[38] German Institute for Standardisation Registered Association, Carbon-based Films and Other Hard Coatings - Rockwell Penetration Test to Evaluate the Adhesion; German Version DIN 4856:2018-02, 2018.
[39] B. Denkena, D. Biermann, Cutting edge geometries, CIRP Ann. 63 (2014) 631–653, https://doi.org/10.1016/j.cirp.2014.05.009.
[40] K.-D. Bouzakis, N. Michailidis, S. Hadjiyiannis, K. Efstathiou, E. Pavlidou, G. Erkens, S. Rambadt, I. Wirth, Improvement of PVD coated inserts cutting performance, through appropriate mechanical treatments of substrate and coating surface, Surf. Coat. Technol. 146-147 (2001) 443–450, https://doi.org/10.1016/S0257-8972(01)01485-2.
[41] C. Schönjahn, M. Bamford, L.A. Donohue, D.B. Lewis, S. Forder, W.-D. Münz, The interface between TiAlN hard coatings and steel substrates generated by high energetic Cr+ bombardment, Surf. Coat. Technol. 125 (2000) 66–70, https://doi.org/10.1016/S0257-8972(99)00552-6.
[42] B. Denkena, B. Breidenstein, Residual stress distribution in PVD-coated carbide cutting tools – origin of cohesive damage, Tribology in Industry (2012) 158–165.
[43] J. Yang, M. Odén, M.P. Johansson-Jõesaar, L. Llanes, Grinding effects on surface integrity and mechanical strength of WC-Co cemented carbides, Procedia CIRP 13 (2014) 257–263, https://doi.org/10.1016/j.procir.2014.04.044.
[44] J. Yang, M. Odén, M.P. Johansson-Jõesaar, J. Esteve, L. Llanes, Mechanical strength of ground WC-Co cemented carbides after coating deposition, Mater. Sci. Eng. A 689 (2017) 72–77, https://doi.org/10.1016/j.msea.2017.02.034.
[45] B. Breidenstein, B. Denkena, Significance of residual stress in PVD-coated carbide cutting tools, CIRP Ann. 62 (2013) 67–70, https://doi.org/10.1016/j.cirp.2013.03.101.
[46] E. Bassett, J. Köhler, B. Denkena, On the honed cutting edge and its side effects during orthogonal turning operations of AISI1045 with coated WC-Co inserts, CIRP J. Manuf. Sci. Technol. 5 (2012) 108–126, https://doi.org/10.1016/j.cirpj.2012.03.004.
[47] C. Cappellini, A. Abeni, A. Attanasio, Modelling of micro-milling by considering tool run-out and ploughing regime, Procedia CIRP 118 (2023) 402–407, https://doi.org/10.1016/j.procir.2023.06.069.
[48] B. Denkena, J.C. Becker, L. de Léon-Gárcia, Study of the influence of the cutting edge microgeometry on the cutting forces and Wear behavior in turning operations, in: R. Neugebauer (Ed.), 8 CIRP International Workshop on Modeling of Machining Operations: Proceedings, May 10–11, 2005, Chemnitz, Germany, Verl. Wiss. Scripten, Zwickau, 2005.